

Fig. 20. Spectral and diffusion distances computed using the Laplacian, Steklov, and volumetric Laplacian spectra. For the bunny, note that the lack of surface monotonicity is the correct and expected behavior for volume distances, including the Steklov and volumetric Laplacian distances.

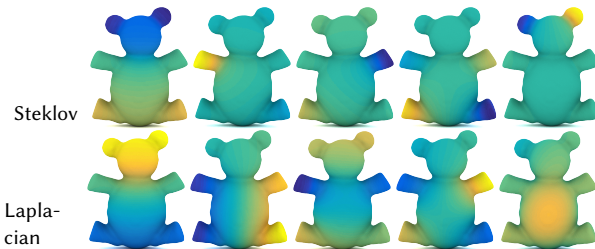


Fig. 21. The Steklov eigenfunctions corresponding to the smallest five non-zero Steklov eigenvalues, with comparison to surface Laplacian eigenfunctions. Note that the Steklov eigenfunctions align with the local extrema of mean curvature, suggesting its use as a segmentation cue.

strategy yields consistent segmentations: While the Laplacian embedding tends to segment the surface into flat patches, the Steklov embedding tends to segment the shape into volumetric parts.

7.5 Shape differences and variability

Rustamov et al. [2013] introduce a notion of shape differences based on an area-based inner product $b^a(u, v) = \langle u, v \rangle_\Gamma$ and a conformal inner product $b^c(u, v) = \langle \nabla_\Gamma u, \nabla_\Gamma v \rangle_\Gamma$ between surface functions u and v .

Similarly, we introduce a volume-aware inner product $b^s(u, v) := \langle \nabla \mathcal{E}u, \nabla \mathcal{E}v \rangle_\Omega$. Superficially this again could be viewed as a substitution of the Laplacian L used for intrinsic shape differences with the DtN operator S . After discretization, this new inner product induces a shape difference operator $D = S_M^{-1} F^\top S_N F$ given a functional map taking functions on the source \mathcal{M} to functions on the target \mathcal{N} . This shape difference operator modifies the function f such that, under the map F the Dirichlet energy $h(f, f)$ of f 's harmonic extension, will be best preserved in the sense $|b_M^s(f, f) - b_N^s(Ff, Ff)|$ is minimized. The action of D reflects how different the two geometric domains are. Inherited from the DtN operator, D defines a more rigid notion of shape differences that captures extrinsic shape changes not captured by intrinsic differences.

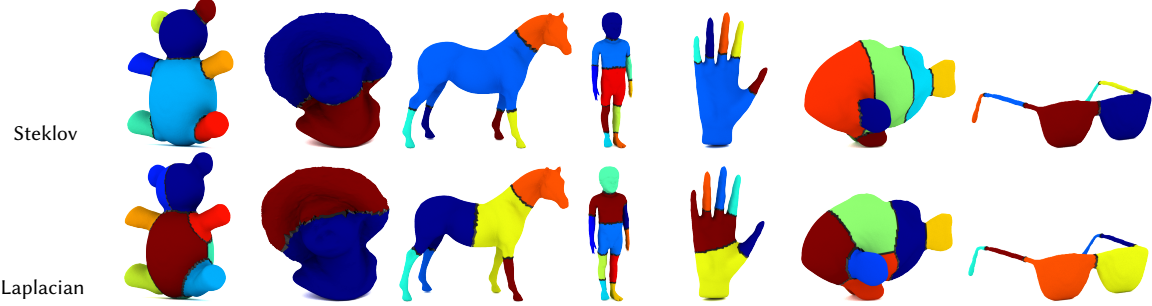


Fig. 22. Results of segmentation by the Steklov and Laplacian embeddings.

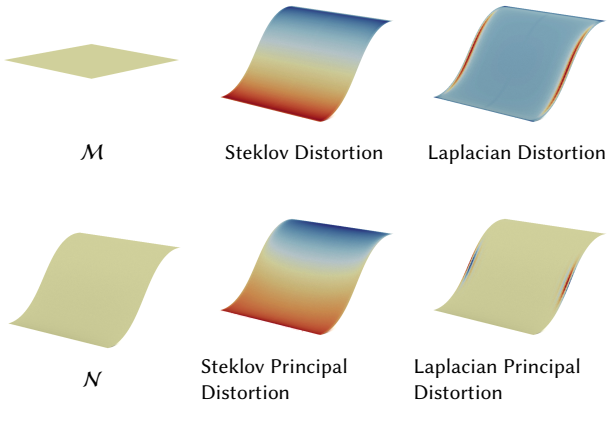


Fig. 23. Point-wise distortion, as well as principal distortion (top singular vector of shape difference operator) measured by the Steklov-based and Laplacian-based shape difference operators for a bending sheet of paper.



Fig. 24. Point-wise distortion measured by the Steklov-based and Laplacian-based shape difference operators. Our Steklov-based operator distinguishes bending direction of the cigar.

For example, Figure 23 shows a shape difference between a rectangular sheet and a bent one, Figure 24 shows a shape difference between a cigar and a bent cigar. The point-wise distortion is measured by the metric

$$(\text{distortion})_i = \frac{\mathbf{e}_i^T \mathbf{M} \mathbf{e}_i}{\mathbf{e}_i^T \mathbf{M} \mathbf{D} \mathbf{e}_i},$$

as in [Rustamov et al. 2013]. The Steklov-based shape difference is far less noisy and distinguishes the bending direction.

Figures 25 illustrate the effect of principal component analysis (PCA) on a collection of shape differences measured through correspondence to a base mesh; see [Rustamov et al. 2013] for details of the technique. Our new difference operator captures the extrinsic changes between surfaces that are nearly identical intrinsically,

most notably the “bumpy cubes” as an extreme example. In general, our Steklov-based shape difference matrices capture more variability in the shape collections than the Laplace–Beltrami counterparts, even when using the generalized DtN operator introduced in §5.5 to study differences between open surfaces (the bending sheet and falling cloth sequences).

7.6 Shape exploration and retrieval

In shape retrieval applications, we may wish to distinguish the same piece of geometry in different poses, e.g. for purposes of organizing a database of human scans or for processing an animated sequence of an articulated character. In these instances, the additional discriminative features provided by DtN-based computation may be desirable. As an example, Figure 26 shows an eigenspace embedding of a collection of shapes from the TOSCA dataset [Bronstein et al. 2008] using the Steklov spectrum, similar to [Reuter et al. 2006].

7.7 Comparison with the Dirac operator

We next compare our method with the Dirac operator [Liu et al. 2017]. From a high level, the DtN operator is assembled using pairwise distances and relative normals, while the relative Dirac operator compares normals of nearby vertices. We highlight differences between the DtN and the Dirac operators here.

Broadly speaking, the Steklov spectrum, like the Laplacian spectrum, considers local geometric details as middle- and high-frequency geometric information; the low eigenvalues are robust (nearly invariant) to such patterns. In contrast, the low end of relative Dirac spectrum detects and discriminates such geometric details.

We provide an experiment in Figure 27 to illustrate this difference. In this example, we take a smooth bowl model and reflect the inward bump outwards to yield an isometric shape; then, we paint noise, smooth clay, and bumps with sharp edges onto the two smooth “bowls”, to create four different types of geometric details. We compute both the Steklov spectrum and the Dirac spectrum on these eight shapes as shown in Figure 27a. In our experiments, the Dirac spectrum is computed using the source code released by the authors, which computes the spectrum of the blended operator of the relative Dirac operator (whose weight is $\sigma = 1 - 10^{-6}$) and the Laplacian operator (whose weight is $1 - \sigma = 10^{-6}$).

The top Steklov eigenvalues in our experiment roughly cluster into two categories, according to whether the bump—a large-scale volumetric feature—points inward or outward. The separation

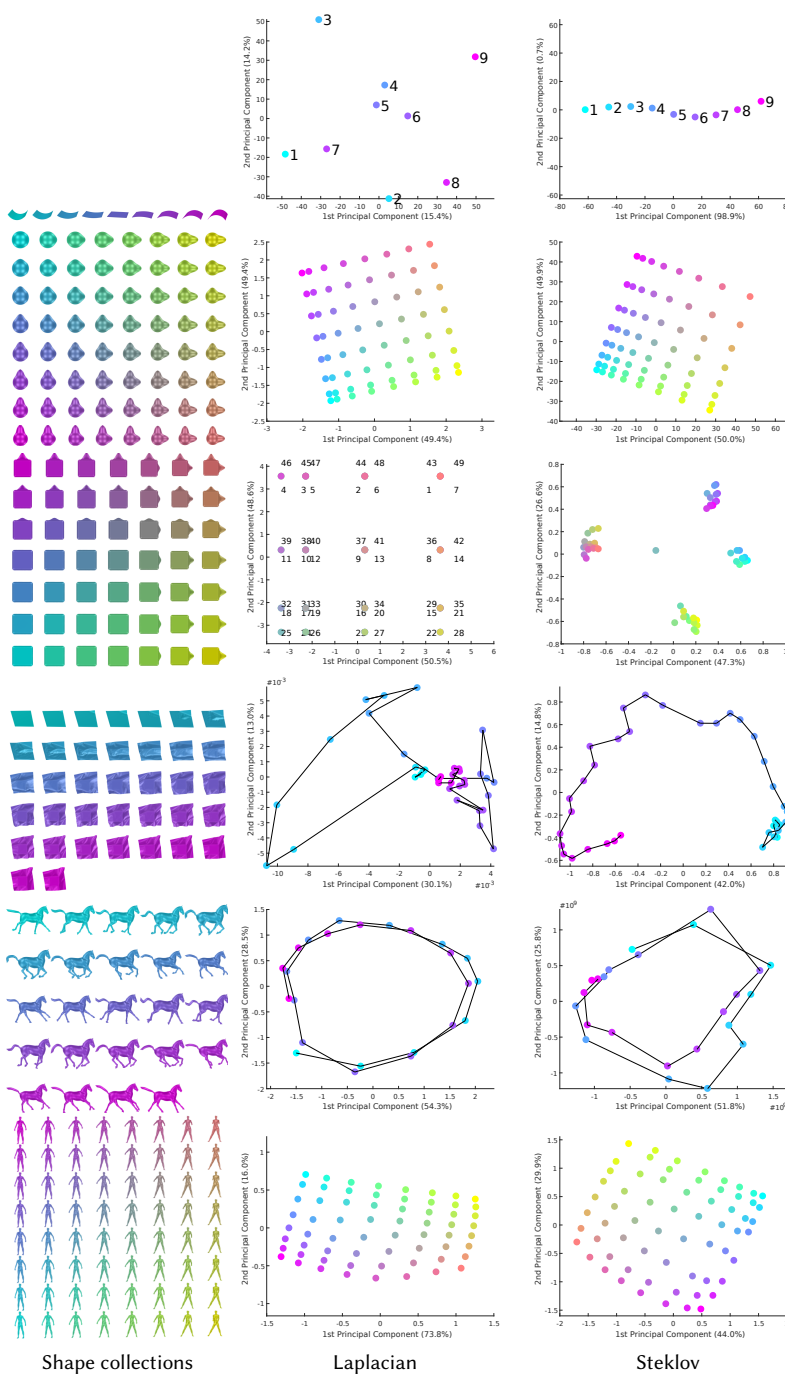
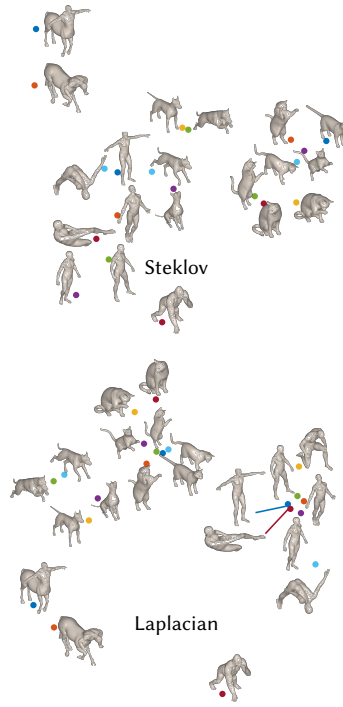
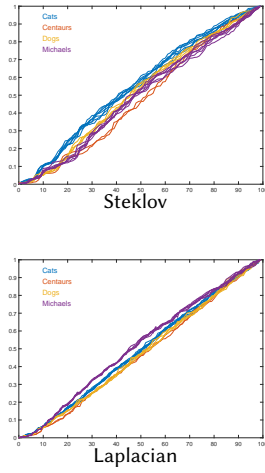


Fig. 25. PCA on collections of shape differences. The Steklov-based shape difference reveals extrinsic deformation that conformal (Laplacian-based) shape difference fails to capture. For the bumpy cube array, the Steklov-based shape difference operator successfully classifies all shapes into four clusters: inward and inward bumps, inward and outward bumps, outward and inward bumps, as well as outward and outward bumps.

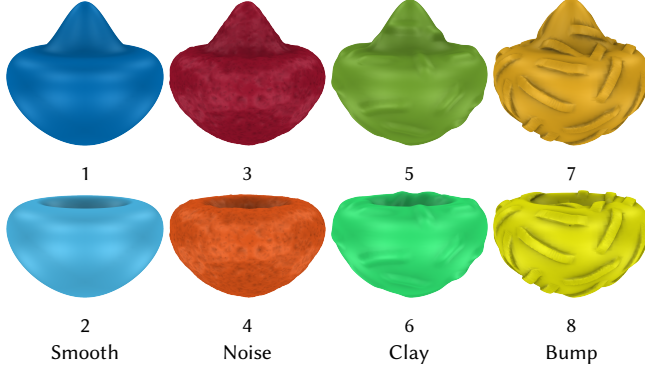


(a) 2D PCA plot of “ShapeDNAs” computed using Steklov and Laplacian eigenvalues. Shapes from the same category tend to cluster together.

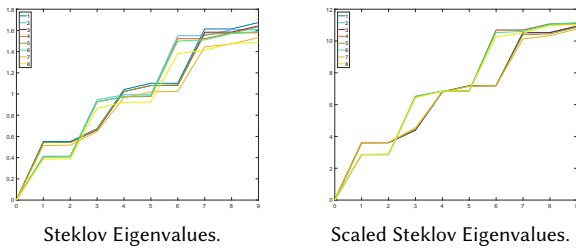


(b) For both Steklov and Laplacian eigenvalues, shapes from the same category have similar eigenvalues; the Steklov spectra cluster correctly but also distinguish between shapes within the same class.

Fig. 26: The Shape “DNA” comparision.



(a) Shapes to compare to [Liu et al. 2017]; the color is used to identify the shape in the following eigenvalue plots.



(c) The top 10 Steklov eigenvalues cluster bowls into two categories, according to whether the bump is inward or outward. Scaling the eigenvalues with the scaling factor $\mathcal{R}(\Omega)$ (defined in Appendix A) makes the separation more clear.

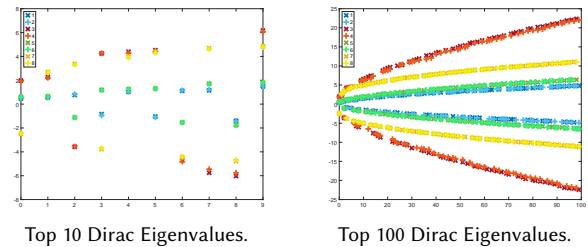
Fig. 27. Comparison with [Liu et al. 2017].

is even more clear after we scale the Steklov eigenvalues using the isoperimetric ratio of each shape, taking into account that the scale of the shape has changed when adding geometric details. The Steklov eigenvalues gradually discriminate geometric details: The spectra of the bumpy, smooth, and noisy bowls start deviating at the 20th, 40th, and 200th eigenvalues, resp. The principal part of the Dirac spectrum, on the other hand, discriminates the shapes into four categories, according to the type of the geometric details. Note the eight shapes are nearly isometric to each other, so adjusting the weighting σ for operator blending does not help discriminate the direction of the bump.

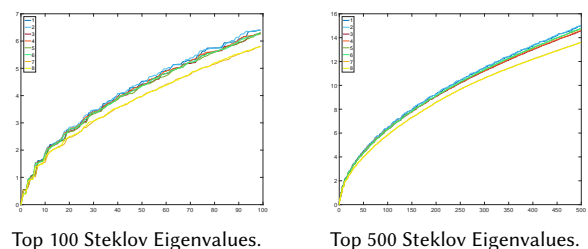
The choice of using Dirac or Steklov depends on the desired behavior of the operator. The Steklov operator captures volumetric information while the Dirac operator is surface-based and accompanied by fewer guarantees. On the other hand, computing the Dirac spectrum involves sparse linear algebra, which can be cheaper than working with the dense BEM system. Geometric details, encoded at the beginning of the Dirac spectrum, are cheaper to obtain from the Dirac spectrum than from the Steklov spectrum.

8 CONCLUSION

The Dirichlet-to-Neumann operator provides an intuitive way to transfer the successes of intrinsic geometry processing to applications needing volumetric information. As we demonstrate using



(b) The top 10 and 100 Dirac eigenvalues (which can be negative). Bowls with the same geometric details have very similar eigenvalues.



(d) The top 100 and 500 Steklov eigenvalues. The eigenvalues eventually go into four classes according to the type of geometric detail.

assorted applications in §7, DtN operators can substitute for Laplace–Beltrami operators *mutatis mutandis* to incorporate extrinsic geometry into existing algorithms and pipelines. The end result is an easily-applied and relatively intuitive extrinsic operator backed by theoretical understanding of its behavior on smooth domains. Our experiments further demonstrate that the boundary integral formulation of the DtN operator appears to encode meaningful geometric data on surfaces with boundary that may not enclose a volumetric region.

The DtN operator is best understood for smooth surfaces. For non-smooth surfaces including ones with sharp structures, theoretical understanding of how the Steklov spectrum is determined by the geometry is an active topic in spectral geometry [Girouard et al. 2017; Levitin et al. 2017]. In addition, numerically computing the spectrum to a high accuracy for these shapes is also a very challenging problem: The inverse single layer potential operator often yields singularities at sharp corners and edges (if the shape contains any; see e.g. [Jackson 1998, §2.11]), leading to less accurate solutions; when fast convergence and high accuracy are desirable one might want to combine our BEM scheme with more sophisticated numerical techniques like [Igarashi and Honma 1996; Lintner and Bruno 2015], to cancel out singularities and end up with a better conditioned system. Our technique as it currently is implemented exhibits some limitations whose resolution will expand the applicability of our work. Most prominently, basic BEM algorithms can

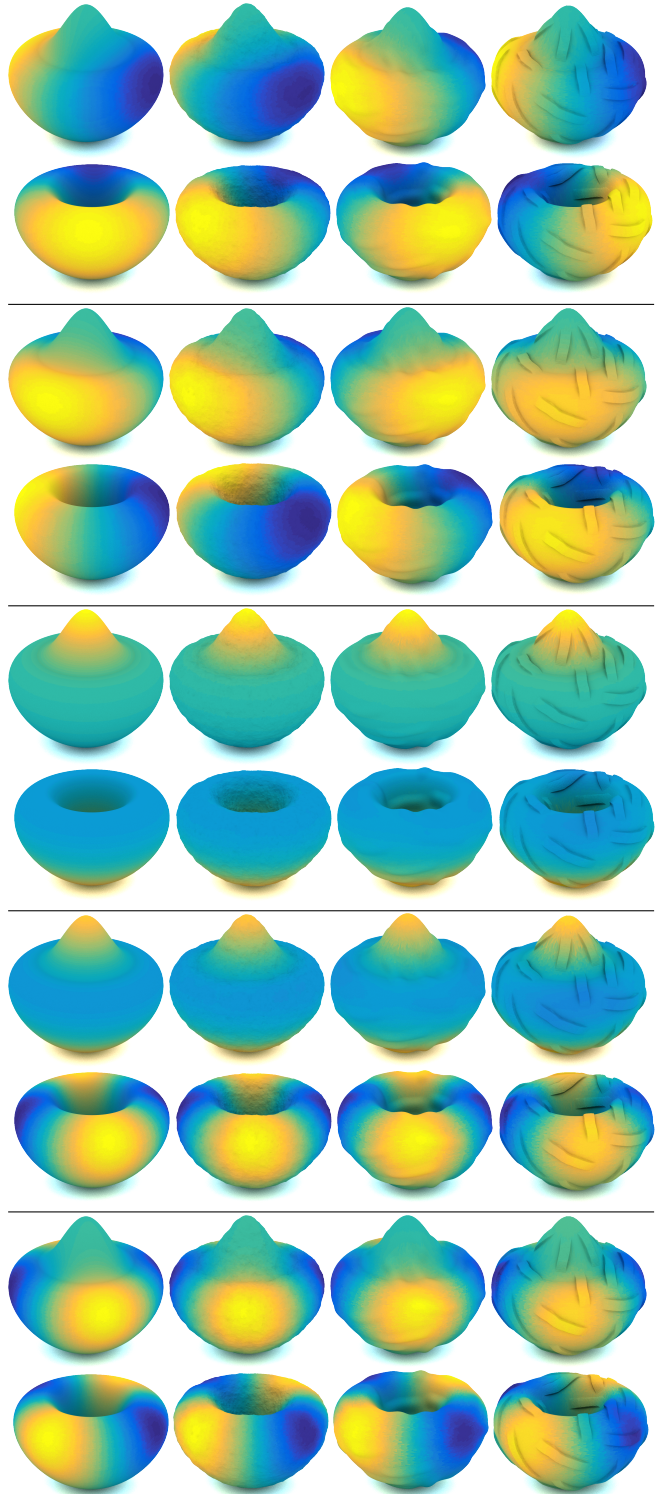


Fig. 28. Steklov eigenfunctions 2–6 computed on the eight shapes. We skipped the first eigenfunction, which is trivially a constant function for all shapes. The eigenfunctions are nearly invariant to geometric detail, though the “rotation” within each eigenspace can be affected.

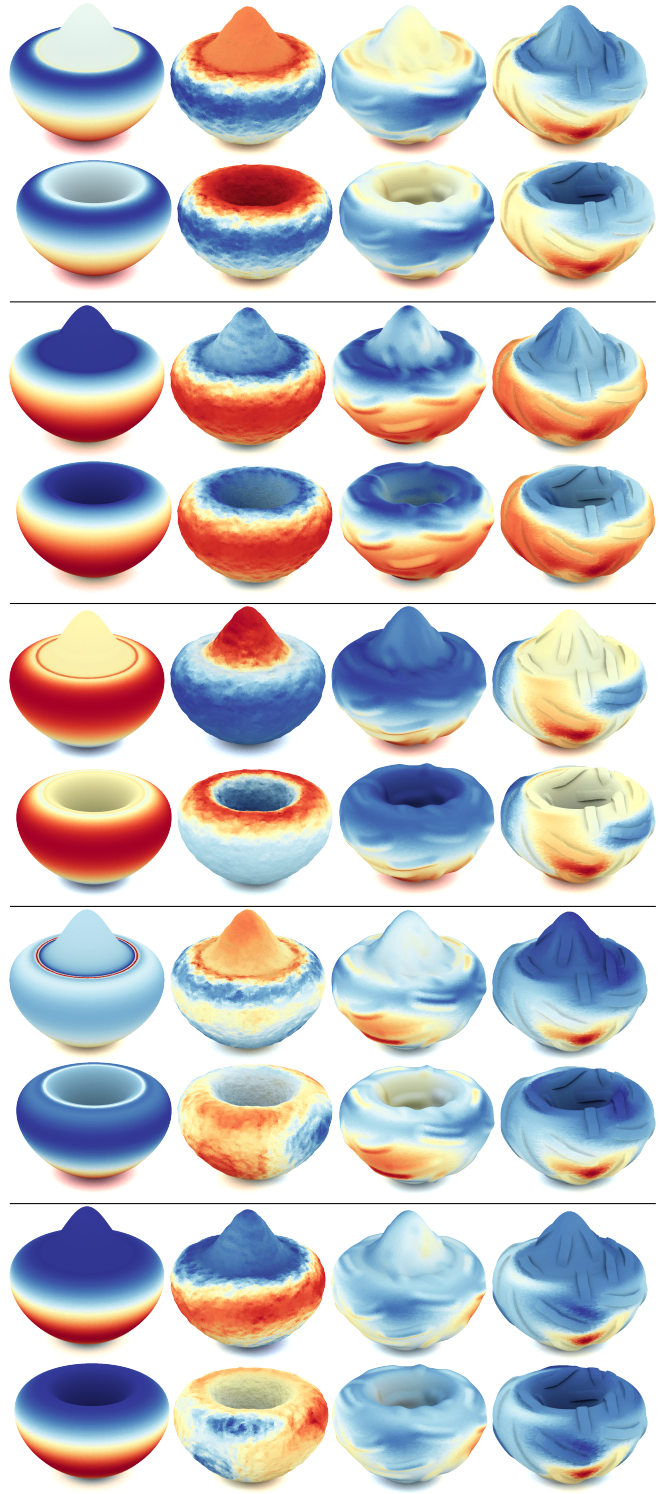


Fig. 29. Magnitudes of the first five (quaternion-valued) Dirac eigenfunctions. We can observe that the eigenfunction resonates most at nearly-flat plateaus and aligns to the clay ridges.

fail when triangle meshes self-overlap, e.g. if two triangles intersect. This drawback potentially can be resolved using a more complex implementation that detects and resolves self-overlap before evaluating boundary integrals, e.g. using techniques recently introduced to the graphics community by Zhou et al. [2016]. Another smaller drawback of our work is the assumption that volumes enclosed by surfaces are homogeneous. In physically-motivated contexts, it may be useful to incorporate anisotropy via modified Laplacian operators or by warping of the interior of the domain. This can be challenging using the boundary element method, which requires closed-form Green’s functions for the differential operators involved.

These potential extensions aside, future work on the computational side might focus on the efficiency of our technique. While asymptotically BEM matches if not surpasses the efficiency of FEM, our current BEM implementation could benefit from accelerated schemes for numerical quadrature and hierarchical matrix evaluation to bring this efficiency to practice. Additional speed could be gained by considering GPU-based implementations of BEM and eigenvalue algorithms, including the GPU-accelerated version of LOBPCG proposed in [Anzt et al. 2015]; their blocked matrix-vector product has some rough similarity to the hierarchical matrix method used in our BEM implementation. GPU-accelerated BEM has been considered in several recent works including [Hamada 2011; Stock and Gharakhani 2010; Takahashi and Hamada 2009; Yokota et al. 2011], a developing topic in numerical analysis that will improve the practical aspects of our method as a side effect. Application-wise, this paper focuses on empirical study of low-level geometric behaviors of the DtN operator and Steklov spectrum; exploring its use in high-level tasks and combining it with the existing techniques in Laplacian geometry processing are interesting directions for future work.

More broadly, our experiments with DtN operators and the Steklov eigenvalue problem reveal the value of considering extrinsic shape in geometry processing pipelines. This and other future approaches will bring a *complete* geometric characterization to the constellation of spectral and operator-based shape processing techniques.

ACKNOWLEDGEMENTS

The authors thank Mikhail Karpukhin for communicating the proof of Proposition 3.1, as well as Chris Wojtan and David Hahn for early conversations about BEM. J. Solomon acknowledges funding from an MIT Skoltech Seed Fund grant (“Boundary Element Methods for Shape Analysis”) and from the MIT Research Support Committee (“Structured Optimization for Geometric Problems”), as well as Army Research Office grant W911NF-12-R-0011 (“Smooth Modeling of Flows on Graphs”). I. Polterovich acknowledges the support of NSERC, FRQNT, the Canada Research Chairs program, as well as the Weston Visiting Professorship program of the Weizmann Institute of Science where part of this research was performed. M. Ben-Chen acknowledges funding from the European Research Council (ERC starting grant No. 714776 “OPREP”), and the Israel Science Foundation (grant No. 504/16). Y. Wang acknowledges the support of MIT Grier Presidential Fellowship and Siebel Scholarship. Meshes are courtesy of the AIM@Shape Repository, the TOSCA project, the

Stanford Computer Graphics Laboratory, MIT, and the Princeton Segmentation Benchmark.

REFERENCES

- Yonathan Afalo, Haim Brezis, and Ron Kimmel. 2015. On the optimality of shape and data representation in the spectral domain. *SIAM Journal on Imaging Sciences* 8, 2 (2015), 1141–1160.
- Hartwig Anzt, Stanimire Tomov, and Jack Dongarra. 2015. Accelerating the LOBPCG method on GPUs using a blocked Sparse Matrix Vector Product. In *Proc. Symposium on High Performance Computing*. 75–82.
- Mathieu Aubry, Ulrich Schlickewei, and Daniel Cremers. 2011. The wave kernel signature: A quantum mechanical approach to shape analysis. In *Proc. ICCV Workshops*. 1626–1633.
- Omri Azencot, Mirela Ben-Chen, Frédéric Chazal, and Maks Ovsjanikov. 2013. An operator approach to tangent vector field processing. In *Computer Graphics Forum*, Vol. 32. 73–82.
- Omri Azencot, Maks Ovsjanikov, Frédéric Chazal, and Mirela Ben-Chen. 2015. Discrete Derivatives of Vector Fields on Surfaces—An Operator Approach. *Transactions on Graphics* 34, 3 (2015), 29.
- Omri Azencot, Orestis Vantzos, and Mirela Ben-Chen. 2016. Advection-Based Function Matching on Surfaces. In *Computer Graphics Forum*, Vol. 35. 55–64.
- Omri Azencot, Steffen Weißmann, Maks Ovsjanikov, Max Wardetzky, and Mirela Ben-Chen. 2014. Functional fluids on surfaces. In *Computer Graphics Forum*, Vol. 33. 237–246.
- Mikhail Belkin, Jian Sun, and Yusu Wang. 2008. Discrete Laplace operator on meshed surfaces. In *Proc. SODA*. 278–287.
- Mikhail Belkin, Jian Sun, and Yusu Wang. 2009. Constructing Laplace operator from point clouds in \mathbb{R}^d . In *Proc. SODA*. 1031–1040.
- Michele Benzi, Gene H Golub, and Jörg Liesen. 2005. Numerical solution of saddle point problems. *Acta Numerica* 14 (2005), 1–137.
- S Bertoluzza. 2003. Non conforming domain decomposition: the Steklov–Poincaré operator point of view. In *Domain Decomposition Methods in Science and Engineering*. 15–26.
- Steffen Börm, Lars Grasedyck, and Wolfgang Hackbusch. 2003. *Hierarchical matrices*. Technical Report. Max Planck Institute.
- Davide Boscaini, Davide Eynard, Drosos Kourounis, and Michael M Bronstein. 2015. Shape-from-Operator: Recovering Shapes from Intrinsic Operators. In *Computer Graphics Forum*, Vol. 34. 265–274.
- James H Bramble and Joseph E Pasciak. 1988. A preconditioning technique for indefinite systems resulting from mixed approximations of elliptic problems. *Math. Comp.* 50, 181 (1988), 1–17.
- Haim Brezis. 2010. *Functional analysis, Sobolev spaces and partial differential equations*. Springer Science & Business Media.
- Alexander M Bronstein, Michael M Bronstein, Leonidas J Guibas, and Maks Ovsjanikov. 2011. Shape Google: Geometric words and expressions for invariant shape retrieval. *Transactions on Graphics* 30, 1 (2011), 1.
- Alexander M Bronstein, Michael M Bronstein, and Ron Kimmel. 2008. *Numerical geometry of non-rigid shapes*. Springer Science & Business Media.
- Oscar P Bruno and Stéphane K Lintner. 2013. A high-order integral solver for scalar problems of diffraction by screens and apertures in three-dimensional space. *J. Comput. Phys.* 252 (2013), 250–274.
- John Canny and John Reif. 1987. New lower bound techniques for robot motion planning problems. In *Annual Symposium on Foundations of Computer Science*. 49–60.
- Xiaobai Chen, Aleksey Golovinskiy, and Thomas Funkhouser. 2009. A benchmark for 3D mesh segmentation. In *Transactions on Graphics*, Vol. 28. ACM, 73.
- Ming Chuang, Linjie Luo, Benedict J Brown, Szymon Rusinkiewicz, and Michael Kazhdan. 2009. Estimating the Laplace–Beltrami Operator by Restricting 3D Functions. In *Computer Graphics Forum*, Vol. 28. 1475–1484.
- Ronald R Coifman and Stéphane Lafon. 2006. Diffusion maps. *Applied and Computational Harmonic Analysis* 21, 1 (2006), 5–30.
- Bruno Colbois, Ahmad El Soufi, and Alexandre Girouard. 2011. Isoperimetric control of the Steklov spectrum. *Journal of Functional Analysis* 261, 5 (2011), 1384–1399.
- Etienne Corman, Justin Solomon, Mirela Ben-Chen, Leonidas Guibas, and Maks Ovsjanikov. 2017. Functional Characterization of Intrinsic and Extrinsic Geometry. *Transactions on Graphics* 36, 2 (March 2017), 14:1–14:17.
- Keenan Crane, Clémence Weisschedel, and Max Wardetzky. 2013. Geodesics in heat: A new approach to computing distance based on heat flow. *Transactions on Graphics* 32, 5 (2013), 152.
- Johannes J Duistermaat and Victor W Guillemin. 1975. The Spectrum of Positive Elliptic Operators and Periodic Bicharacteristics. *Inventiones Mathematicae* 29 (1975), 39–80.
- Nader Engheta, William D Murphy, Vladimir Rokhlin, and Marius S Vassiliou. 1992. The fast multipole method (FMM) for electromagnetic scattering problems. *Transactions on Antennas and Propagation* 40, 6 (1992), 634–641.
- Ming Gao, Nathan Mitchell, and Eftychios Sifakis. 2014. Steklov–Poincaré skinning. In *Proc. Symposium on Computer Animation*. 139–148.

- Alexandre Girouard, Jean Lagacé, Iosif Polterovich, and Alessandro Savo. 2017. The Steklov spectrum of cuboids. *arXiv preprint arXiv:1711.03075* (2017).
- Alexandre Girouard and Iosif Polterovich. 2017. Spectral geometry of the Steklov problem. *J. Spectral Theory* 7, 2 (2017), 321–359.
- Gerd Grubb. 2009. *Pseudodifferential methods for boundary value problems*. 305–333.
- Wolfgang Hackbusch. 1999. A sparse matrix arithmetic based on \mathcal{H} -matrices. Part I: Introduction to \mathcal{H} -matrices. *Computing* 62, 2 (1999), 89–108.
- Shoji Hamada. 2011. GPU-accelerated indirect boundary element method for voxel model analyses with fast multipole method. *Computer Physics Communications* 182, 5 (2011), 1162–1168.
- Klaus Hildebrandt, Christian Schulz, Christoph von Tycowicz, and Konrad Polthier. 2010. Eigenmodes of Surface Energies for Shape Analysis.. In *GMP*. Springer, 296–314.
- Hugues Hoppe. 1996. Progressive meshes. In *Proc. SIGGRAPH*, 99–108.
- Hajime Igarashi and Toshihisa Honma. 1996. A boundary element method for potential fields with corner singularities. *Applied mathematical modelling* 20, 11 (1996), 847–852.
- John David Jackson. 1998. Classical Electrodynamics. *Classical Electrodynamics, 3rd Edition*, by John David Jackson, pp. 832. ISBN 0-471-30932-X. Wiley-VCH, July 1998. (1998), 832.
- Alec Jacobson. 2013. *Algorithms and interfaces for real-time deformation of 2d and 3d shapes*. Ph.D. Dissertation. ETH Zurich.
- Alec Jacobson, Ladislav Kavan, and Olga Sorkine-Hornung. 2013. Robust inside-outside segmentation using generalized winding numbers. *ACM Transactions on Graphics (TOG)* 32, 4 (2013), 33.
- Alexander Kachalov, Yaroslav Kurylev, and Matti Lassas. 2001. *Inverse boundary spectral problems*. CRC Press.
- Ram P Kanwal. 2013. *Linear integral equations*. Springer.
- Andrew V Knyazev. 2001. Toward the optimal preconditioned eigensolver: Locally optimal block preconditioned conjugate gradient method. *SIAM Journal on Scientific Computing* 23, 2 (2001), 517–541.
- Iasonas Kokkinos, Michael M Bronstein, Roee Litman, and Alex M Bronstein. 2012. Intrinsic shape context descriptors for deformable shapes. In *Proc. CVPR*, 159–166.
- John M Lee and Gunther Uhlmann. 1989. Determining anisotropic real-analytic conductivities by boundary measurements. *Communications on Pure and Applied Mathematics* 42, 8 (1989), 1097–1112.
- Michael Levitin, Leonid Parnovsky, Iosif Polterovich, and David A Sher. 2017. Sloshing, Steklov and corners I: Asymptotics of sloshing eigenvalues. *arXiv preprint arXiv:1709.01891* (2017).
- Jian Liang, Rongjie Lai, Tsz Wai Wong, and Hongkai Zhao. 2012. Geometric understanding of point clouds using Laplace–Beltrami operator. In *Proc. CVPR*, 214–221.
- Stéphane K Lintner and Oscar P Bruno. 2015. A generalized Calderón formula for open-arc diffraction problems: theoretical considerations. *Proceedings of the Royal Society of Edinburgh Section A: Mathematics* 145, 2 (2015), 331–364.
- Yaron Lipman, Raif M Rustamov, and Thomas A Funkhouser. 2010. Biharmonic distance. *Transactions on Graphics* 29, 3 (2010), 27.
- Roee Litman, Alexander M Bronstein, and Michael M Bronstein. 2012. Stable volumetric features in deformable shapes. *Computers & Graphics* 36, 5 (2012), 569–576.
- Haixiang Liu, Nathan Mitchell, Mridul Aanjaneya, and Eftychios Sifakis. 2016. A scalable Schur-complement fluids solver for heterogeneous compute platforms. *Transactions on Graphics* 35, 6 (2016), 201.
- Hsueh-Ti Derek Liu, Alec Jacobson, and Keenan Crane. 2017. A Dirac operator for extrinsic shape analysis. In *Computer Graphics Forum*, Vol. 36. Wiley Online Library, 139–149.
- Robert Osada, Thomas Funkhouser, Bernard Chazelle, and David Dobkin. 2002. Shape distributions. *Transactions on Graphics* 21, 4 (2002), 807–832.
- Maks Ovsjanikov, Mirela Ben-Chen, Justin Solomon, Adrian Butscher, and Leonidas Guibas. 2012. Functional maps: a flexible representation of maps between shapes. *Transactions on Graphics* 31, 4 (2012), 30.
- Giuseppe Patané. 2015. Volumetric heat Kernel: Padé–Chebyshev approximation, convergence, and computation. *Computers & Graphics* 46 (2015), 64–71.
- Giuseppe Patané. 2016. Laplacian Spectral Kernels and Distances for Geometry Processing and Shape Analysis. In *Computer Graphics Forum*, Vol. 35. 599–624.
- Ulrich Pinkall and Konrad Polthier. 1993. Computing discrete minimal surfaces and their conjugates. *Experimental Mathematics* 2, 1 (1993), 15–36.
- Iosif Polterovich and David A Sher. 2015. Heat invariants of the Steklov problem. *The Journal of Geometric Analysis* 25, 2 (2015), 924–950.
- Alfio Quarteroni and Alberto Valli. 1999. *Domain decomposition methods for partial differential equations*. Oxford.
- Dan Raviv, Michael M Bronstein, Alexander M Bronstein, and Ron Kimmel. 2010. Volumetric heat kernel signatures. In *Proc. 3DOR*, 39–44.
- Martin Reuter, Silvia Biasotti, Daniela Giorgi, Giuseppe Patanè, and Michela Spagnuolo. 2009. Discrete Laplace–Beltrami operators for shape analysis and segmentation. *Computers & Graphics* 33, 3 (2009), 381–390.
- Martin Reuter, Franz-Erich Wolter, and Niklas Peinecke. 2006. Laplace–Beltrami spectra as ‘Shape-DNA’ of surfaces and solids. *Computer-Aided Design* 38, 4 (2006), 342–366.
- Vladimir Rokhlin. 1985. Rapid solution of integral equations of classical potential theory. *J. Comput. Phys.* 60, 2 (1985), 187–207.
- Raif M Rustamov. 2011. Interpolated eigenfunctions for volumetric shape processing. *The Visual Computer* 27, 11 (2011), 951–961.
- Raif M Rustamov, Maks Ovsjanikov, Omri Azencot, Mirela Ben-Chen, Frédéric Chazal, and Leonidas Guibas. 2013. Map-based exploration of intrinsic shape differences and variability. *Transactions on Graphics* 32, 4 (2013), 72.
- Rohan Sawhney and Keenan Crane. 2017. Boundary First Flattening. *ACM Transactions on Graphics (TOG)* 37, 1 (2017), 5.
- Wojciech Śmigaj, Timo Betcke, Simon Arridge, Joel Phillips, and Martin Schweiger. 2015. Solving boundary integral problems with BEM++. *Transactions on Mathematical Software* 41, 2 (2015), 6.
- Barry Smith, Petter Björstad, and William Gropp. 2004. *Domain decomposition: parallel multilevel methods for elliptic partial differential equations*. Cambridge.
- Olga Sorkine. 2005. Laplacian Mesh Processing. In *Eurographics State of the Art Report*.
- Olaf Steinbach. 2007. *Numerical approximation methods for elliptic boundary value problems: finite and boundary elements*. Springer.
- Olaf Steinbach and Wolfgang L Wendland. 1998. The construction of some efficient preconditioners in the boundary element method. *Advances in Computational Mathematics* 9, 1–2 (1998), 191–216.
- Mark J Stoch and Adrin Gharakhani. 2010. A GPU-accelerated boundary element method and vortex particle method. In *AIAA 40th Fluid Dynamics Conference and Exhibit*, Vol. 1.
- Martin Stoll and AJ Wathen. 2007. *The Bramble–Pasciak preconditioner for saddle point problems*. Technical Report. University of Oxford.
- Jian Sun, Maks Ovsjanikov, and Leonidas Guibas. 2009. A Concise and Provably Informative Multi-Scale Signature Based on Heat Diffusion. In *Computer Graphics Forum*, Vol. 28. 1383–1392.
- Toru Takahashi and Tsuyoshi Hamada. 2009. GPU-accelerated boundary element method for Helmholtz equation in three dimensions. *Internat. J. Numer. Methods Engrg.* 80, 10 (2009), 1295–1321.
- Federico Tombari, Samuele Salti, and Luigi Di Stefano. 2010. Unique signatures of histograms for local surface description. In *Proc. ECCV*, 356–369.
- Andrea Toselli and Olof B Widlund. 2005. *Domain decomposition methods: algorithms and theory*. Vol. 34. Springer.
- Bruno Vallet and Bruno Lévy. 2008. Spectral geometry processing with manifold harmonics. In *Computer Graphics Forum*, Vol. 27. 251–260.
- Amir Vaxman, Mirela Ben-Chen, and Craig Gotsman. 2010. A multi-resolution approach to heat kernels on discrete surfaces. *Transactions on Graphics* 29, 4 (2010), 121.
- Gang Wang and Yalin Wang. 2015. Multi-scale Heat Kernel Based Volumetric Morphology Signature. In *International Conference on Medical Image Computing and Computer-Assisted Intervention*, 751–759.
- Hao Wang, Tong Lu, Oscar Kin-Chung Au, and Chiwei-Lan Tai. 2014. Spectral 3D mesh segmentation with a novel single segmentation field. *Graphical Models* 76, 5 (2014), 440–456.
- Kenong Wu and Martin D Levine. 1997. 3D part segmentation using simulated electrical charge distributions. *IEEE Transactions on Pattern Analysis and Machine Intelligence* 19, 11 (1997), 1223–1235.
- Rio Yokota, Jaydeep P Bardhan, Matthew G Knepley, Lorena A Barba, and Tsuyoshi Hamada. 2011. Biomolecular electrostatics using a fast multipole BEM on up to 512 GPUs and a billion unknowns. *Computer Physics Communications* 182, 6 (2011), 1272–1283.
- Hao Zhang, Oliver Van Kaick, and Ramsay Dyer. 2010. Spectral mesh processing. In *Computer Graphics Forum*, Vol. 29. 1865–1894.
- Qingnan Zhou, Eitan Grinspun, Denis Zorin, and Alec Jacobson. 2016. Mesh Arrangements for Solid Geometry. *Transactions on Graphics* 35, 4 (July 2016), 39:1–39:15.

A EIGENVALUE NORMALIZATION

For shape analysis applications where scale invariance is desired, we suggest using the following isoperimetric-ratio-based scaling factor:

$$\mathcal{R}(\Omega) := \frac{\text{AREA}(\partial\Omega)}{\sqrt[3]{\text{VOL}(\Omega)}},$$

where $\text{AREA}(\partial\Omega)$ and $\text{VOL}(\Omega)$ are surface area and interior volume of the domain Ω . This scaling factor is justified by the following theorem

THEOREM A.1 ([COLBOIS ET AL. 2011, THEOREM 1.3]). *If $\Omega \in \mathbb{R}^3$ is conformally equivalent to a complete manifold with non-negative Ricci curvature, then $\lambda_i(\Omega) \leq c \frac{i^{2/3}}{\mathcal{R}(\Omega)}$, $\forall i$, where c is a constant.*

Note this is not an asymptotic formula. Figure 27 shows that this scaling factor behaves reasonably for that example, cancelling the effects of volume and area scaling.

Volume can be robustly evaluated, even for non-watertight meshes, from a boundary representation as the integral

$$\begin{aligned}\text{Vol}(\Omega) &:= \frac{1}{3} \int_{\Gamma} \mathbf{x} \cdot \mathbf{n}(\mathbf{x}) d\Gamma(\mathbf{x}) \\ &= \frac{1}{18} \sum_{T_i} (\mathbf{x}_{i,1} + \mathbf{x}_{i,2} + \mathbf{x}_{i,3}) \cdot ((\mathbf{x}_{i,3} - \mathbf{x}_{i,2}) \times (\mathbf{x}_{i,2} - \mathbf{x}_{i,1})).\end{aligned}$$

where $\mathbf{x}_{i,\{1,2,3\}}$ are positions of the three vertices in the triangle T_i .